Imaging of Transient Electromagnetic Soundings Using a Scaling Approximate Fréchet Derivative

Niels B. Christensen

Department of Earth Sciences, Aarhus University, Aarhus, Denmark

1 Introduction

Transient electromagnetic (TEM) soundings have found widespread use in a variety of geophysical investigations in connection with environmental problems, hydrogeological investigations, and mineral prospecting (Spies and Frischknecht 1991). Modern strategies of measurement and instrument design emphasize dense measurements covering large areas resulting in vast amounts of data to be interpreted (Christensen and Sørensen 1994, Sørensen et al. 1995, Sørensen 1996). For airborne applications this is carried to the extreme.

Traditionally, TEM soundings have been interpreted with one-dimensional (1D) earth models using an iterative least squares inversion technique to determine layer conductivities and thicknesses (Boerner and West 1989, Raiche et al. 1985). This problem is highly nonlinear making the inversion task considerable even on modern PC's.

An algorithm for 1D approximate inversion, "imaging", of TEM soundings based on the Born approximation and the Fréchet kernel of the homogeneous halfspace is presented. The kernel is scaled according to the average conductivity of the earth for each time of measurement. To a large extent this scaling linearizes the TEM inversion problem, and the use of apparent conductivity as data makes it considerably less dependent on the measurement configuration. In practical calculations simple, piecewise linear approximations to the Fréchet kernel are used resulting in more or less damped inverse operators.

The computation time is approximately 0.5 sec/sounding/Mflop, which is 2-3 orders of magnitude faster than conventional least squares iterative inversion. The imaging produces models with many layers, typically 20-40, which fit the original data typically within 5-15% rms. No initial model is required, and the algorithm is therefore well suited for on-line and automatic inversion as well as for approximate inverse mapping schemes (AIM) (Oldenburg 1991). The imaging provides good initial models for a more rigorous least squares inversion.

The principle of a scaling Fréchet kernel can be extended to the 3D transient case as well as to other types of electromagnetic data.

2 Current distribution and sensitivity function

The current density distribution resulting from a step off at time zero from a vertical magnetic dipole is shown in figure 1a. The current in the ground has only an azimuthal component, and the current maximum diffuses outwards and downwards with time, while the maximum broadens and decreases in amplitude due to ohmic loss in the conductor. The current density maximum follows a straight line, making an angle of approximately 27° with the surface.

The sensitivity of the transient method, however, does not depend directly on the current distribution at depth, but on the effect of the current distribution on the measured field - in our case the vertical magnetic field measured at the center. Using the usual formula for the H-field on the axis of a circular current, the current element situated at the point with the cylindrical coordinates (r, z) contributes to the magnetic field at the surface as

$$dH(\sigma, t) = j(\sigma, t, r, z)\ dr\ dz \times \tfrac{1}{2}\,\frac{r^2}{(r^2+z^2)^{3/2}} \tag{1}$$

where σ is the conductivity, t is time, and $j(\sigma, t, r, z)$ is he current density at (r, z).

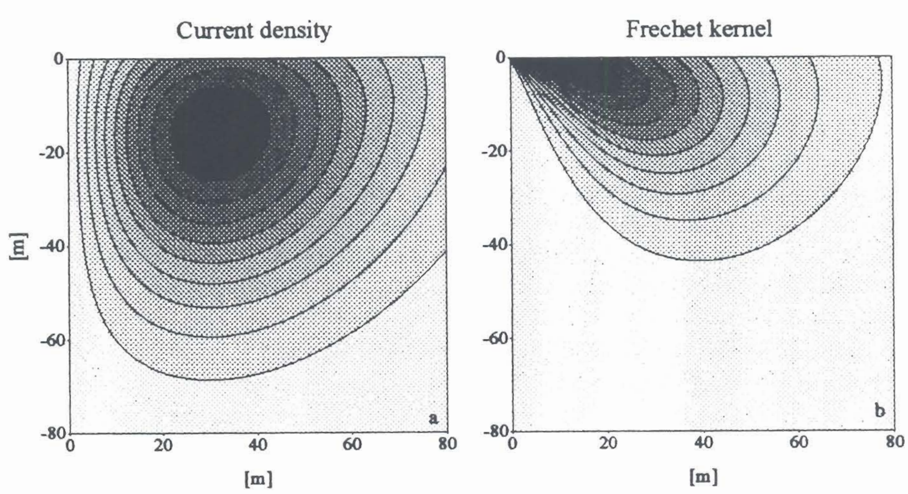

Fig. 1. a: Contoured plot of the current density in the ground 500 μs after turn-off of a vertical magnetic dipole on a 1Ωm homogeneous halfspace. b: Contoured plot of the current density weighted according to its contribution to the vertical H-field at the center (equation 1). Contour intervals are 10% af the maximum value.

Figure 1b shows the current distribution of figure 1a weighted according to its influence on the H-field. This plot reveals some interesting features of the transient method. The sensitivity of the method stays high at the surface close to the center at all times and can be described as a cone-shaped structure, which broadens outwards and downwards with time. The 'ridge' lies along a straight line, making an angle of approximately 15° with the surface. Note also that there is almost no sensitivity to the conductivity distribution within a cone with an opening angle of 30° directly under the source.

In the quasi-stationary case, which is the one considered here, the function described in figure 1b is the 3D rotationally symmetric sensitivity function of the vertical magnetic field with respect to conductivity for the homogeneous halfspace. The Fréchet kernel is identical to this function divided by the conductivity, σ, of the halfspace.

3 The 1D Fréchet kernel

The 1D Fréchet kernel for the homogeneous halfspace can be found by integrating the 3D Fréchet kernel. This results in an analytic expression (Christensen 1995):

$$F(\sigma,t,z) = \frac{M}{4\pi}\,\frac{1}{16\,\sigma\,\tau^4}\left\{\frac{2u}{\sqrt{\pi}}(2u^2+1)\,e^{-u^2} - (4u^4+4u^2-1)\,\mathrm{erfc}(u)\right\} \quad (2)$$

$$= \frac{M}{30\,\pi^{3/2}\,\tau^3}\,\frac{1}{\sigma}\,\tilde{F}(\sigma,t,z)\ ,\quad \tau = \sqrt{t/(\mu\sigma)}\ \text{ and }\ u = z/(2\tau)\ .$$

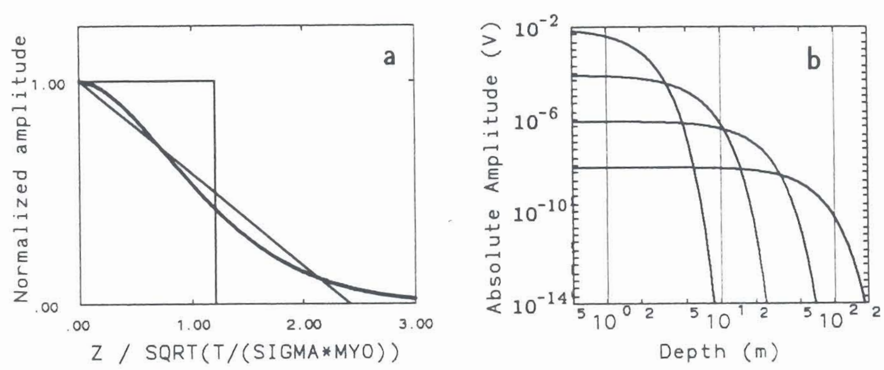

Fig. 2. a: The normalized 1D Fréchet kernel for the transient vertical magnetic dipole in the case of a homogeneous halfspace as a function of normalized depth (thick grey curve) together with the constant and the linear approximations to the Fréchet kernel. b: The unnormalized Fréchet kernel for a halfspace resistivity of 1 Ωm at the times 1 μs, 10 μs, 100 μs, and 1 ms.

Figure 2a shows a plot of $F(\sigma, t)$ on a linear scale and figure 2b shows $F(\sigma, t)$ on a logarithmic scale at four different times for a source dipole of unit moment. It is seen that the sensitivity is a bell-shaped function of z, which has its maximum at the surface at all times. Figure 2b shows how the amplitude decreases and the depth of diffusion increases as a function of time. The sensitivity drops very abruptly to zero with depth, decreasing as $u^{-3}\exp(-u^2)$.

4 The imaging algorithm

Imaging of transient electromagnetic soundings has been the subject of many investigations in the geophysical litterature (e.g. Macnae and Lamontagne 1987, Smith et al. 1994).

The imaging algorithm proposed here is based on the Born approximation and the Fréchet derivative of the homogeneous halfspace. However, instead of choosing a constant reference conductivity of the halfspace, a new reference conductivity is chosen for each time of measurement. This reference conductivity is chosen equal to the instantaneous apparent conductivity of the measurement, which by definition is equal to the halfspace conductivity, which would produce the actual field at the time of the measurement. In this way the slower diffusion of current (relative to the homogeneous halfspace) in good conductors and the faster diffusion through bad conductors is taken into account.

In the approximation that conductivity changes are small, the Born approximation describes the change in the response as a linear functional of the change in subsurface conductivity:

$$H_i \simeq H_i^{ref} + \int_0^{\infty} F\left(\sigma^{ref}(z), t_i, z\right)\left[\sigma(z) - \sigma^{ref}(z)\right] dz \tag{3}$$

where

H_i is the measured H-field at the time t_i.

H_i^{ref} is the H-field of the reference model.

$F(\sigma^{ref}(z), t, z)$ is the Fréchet kernel of the reference model.

$\sigma(z)$ is the conductivity of the subsurface.

$\sigma^{ref}(z)$ is the conductivity of the reference model.

The response of the homogeneous halfspace with conductivity σ^0 is the integral of the Fréchet kernel multiplied with conductivity

$$H_i^0 = \int_0^{\infty} F(\sigma^0, t_i, z)\,\sigma^0\,dz = \frac{M}{30}\left(\frac{\sigma^0\mu}{\pi t}\right)^{3/2} = \frac{M}{30\,\pi^{3/2}}\,\frac{1}{\tau^3}\;. \tag{4}$$

For a measured $H_i(t_i)$ over any 1D structure the solution of equation (4) in terms of σ^0 will give us the apparent conductivity $\sigma^a(t_i)$.

In the case, where the reference model is a homogeneous halfspace, we find

$$H_i \simeq H_i^0 + \int_0^\infty F(\sigma^0, t_i, z)\,(\sigma(z) - \sigma^0)\,dz = \int_0^\infty F(\sigma^0, t_i, z)\,\sigma(z)\,dz \tag{5}$$

For a layered 1D structure with L layers given by the layer boundaries z_i, $i=1, L+1$, $z_1=0$, $z_{L+1} = \infty$, the conductivity is constant within each layer and equation (5) becomes

$$H_i \simeq \sum_{j=1}^{L} \sigma_j \int_{z_j}^{z_{j+1}} F(\sigma^0, t_i, z)\,dz \tag{6}$$

The scaling of the Frechet kernel is obtained by substituting the apparent conductivity $\sigma^a(t_i)$ instead of the constant halfspace conductivity σ^0 in the expresion for the Fréchet kernel in equation (2), and substituting equation (4) in (2) we arrive at:

$$H_i \simeq \sum_{j=1}^{L} \sigma_j \int_{z_j}^{z_{j+1}} F(\sigma^a(t_i), t_i, z)\,dz_i = \sum_{j=1}^{L} \sigma_j \frac{H_i}{\sigma^a(t_i)} \int_{z_j}^{z_{j+1}} \tilde{F}(\sigma^a(t_i). t_i, z)\,dz$$

$$\Rightarrow \qquad \sigma^a(t_i) \simeq \sum_{j=1}^{L} \sigma_j \int_{z_j}^{z_{j+1}} \tilde{F}(\sigma^a(t_i), t_i, z)\,dz\ . \tag{7}$$

Equation (7) expresses the apparent conductivity as a weighted sum of the conductivities of each layer with easily calculated weights.

The problem of damping the inverse is adressed by using a constant and a linear approximation to the Fréchet kernel (fig. 2a) instead of using the exact kernel. The constant approximation results in a well damped inverse, whereas the linear approximation gives a more sensitive "spiked" inverse.

By choosing the surface amplitude of the approximations equal to that of the true kernel and by demanding the integral over the halfspace to be the same as that of the true kernel, the constant approximation is given by

$$\begin{aligned} &F(\sigma, t, z) = F^0 = \frac{M}{4\pi}\frac{1}{16\,\sigma\,\tau^4} = H_i \cdot \frac{15\sqrt{\pi}}{32\,\tau}\frac{1}{\sigma} && \text{for } z < z_D \\ &F(\sigma, t, z) = 0 \quad \text{for } z > z_D \quad , \quad z_D = \frac{32}{15\sqrt{\pi}}\,\tau && \end{aligned} \tag{8}$$

Choosing the layer boundaries z_j equal to the diffusion depths of the Fréchet kernel, z_D, gives a particularly simple version of equation (7)

$$\sigma_i^a = \sum_{j=1}^{i} \sigma_j \frac{h_j}{z_{D_i}} \tag{9}$$

where h_j is the thickness of the j'th layer. Equation (9) may easily be inverted for the layer conductivities by forward substitution. It is a "stripping the earth" algorithm.

The above derivations have all assumed the source and receiver to be coincident vertical magnetic dipoles, which is not a practical measuring configuration. However, equation (7) may be used for other configurations as well, provided that a suitable definition of apparent conductivity can be found with which the Fréchet kernel can be scaled.

Among the many definitions of apparent conductivity, the all-time apparent conductivity based on the step response - the H-field itself - must be chosen. For the central loop and the coincident loop configuration it is unambiguously defined and exists always, as the H-field is a monotonically decreasing function of time, and it has a smooth transition between resistivity levels. The field quantity most often measured with transient equipments is dH/dt, but the apparent conductivity definitions based on dH/dt (Spies 1986) are not applicable. However, given dH/dt data we may calculate the H-field numerically, and from the H-field we can calculate the all-time apparent conductivity as a function of time (Christensen 1995).

The all-time apparent conductivity does not only serve the scaling purpose, but is also used as input data. This parameter is to a much larger extent independent on measuring configuration than the H-field, and so the procedure developed for the vertical magnetic dipole is also applicable for other configurations.

5 Results and discussion

Figure 3 shows the models resulting from the application of the imaging algorithm on synthetic noise-free data from four different models together with the true resistivity models: two 2-layer models (descending and ascending) and two 3-layer models (minimum and maximum). The results for the double descendeing and double descending 3-layer models a similar to the 2-layer models. It is seen that the imaging algorithm works very well with descending type models, but reacts slower to ascending resistivity models. The worst performance is seen with the maximum model, which is to be expected. From the asymptotic behaviour it is seen that the imaged models reach the true value of the resistivity very well.

The constant approximation to the Fréchet kernel results in very little undershoot and overshoot in the imaged models and is thus a more damped inverse, whereas such effects are seen to some extent, if the linear approximation is used.

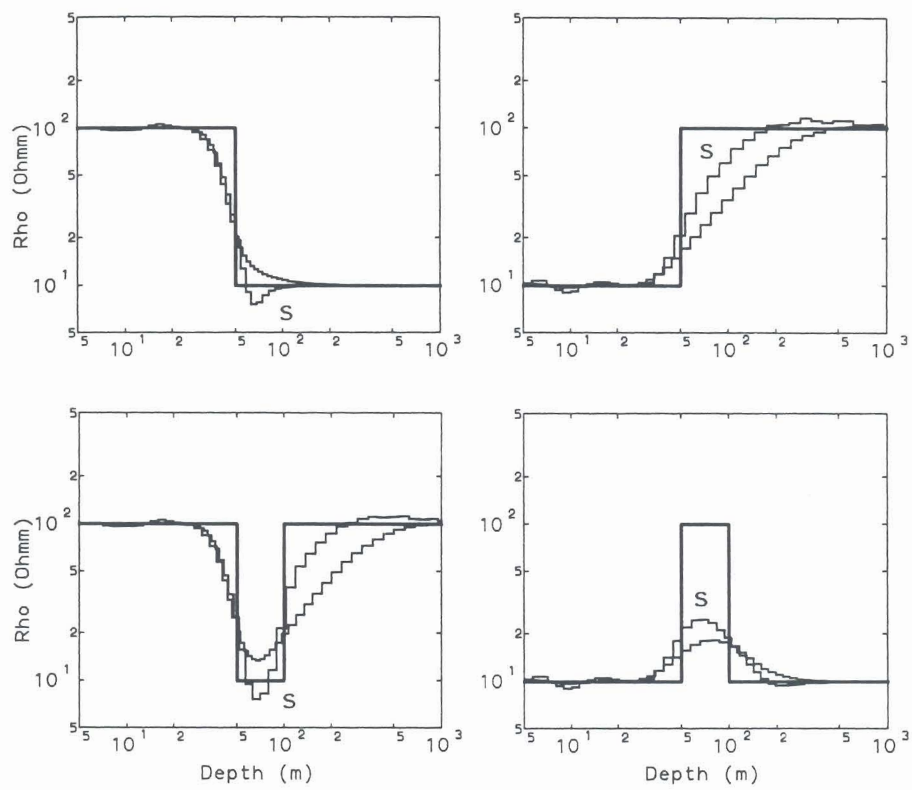

Fig. 3. The models obtained using the imaging procedures on 40×40 m^2 central loop soundings. The figure shows a comparison between the results obtained with the more damped constant approximation and the more sensitive linear approximation to the Fréchet kernel for four models. The true models are shown with thick grey curves. The sensitive inverse is marked with an "S".

The models produced by the imaging procedure fit the original data typically within 5-15% rms and are well-behaved without extreme discrepancies. This is very satisfactory for a one-pass algorithm working almost instantaneously. Two examples are shown in figure 4: the two layer descending and ascending models, representing the best and the worst case among the four models of figure 3, respectively. From dH/dt data the H-field and the all-time apparent conductivity have been calculated and the imaging applied using the constant approximation to the Fréchet kernel.

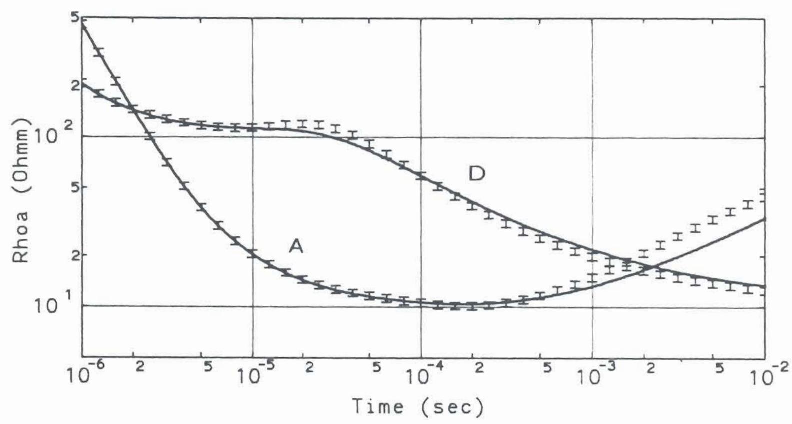

Fig. 4. Comparison between forward responses of imaged models and original data for the two-layer descending (D) and ascending (A) models of figure 3. The rms misfits are 6.9% and 13.3%, respectively.

Figure 5 shows the application of the imaging algorithm to a profile of transient soundings in the central loop configuration. The result of the imaging is displayed as a contoured model section. The profile is from the island of Rømø, Denmark, where it transects the NE corner of the island. The good conductor - the salt water horizon - is closer to the surface at the ends of the profile, where the distance to the coast is small and lies deeper in the middle of the profile, which is situated furher inland.

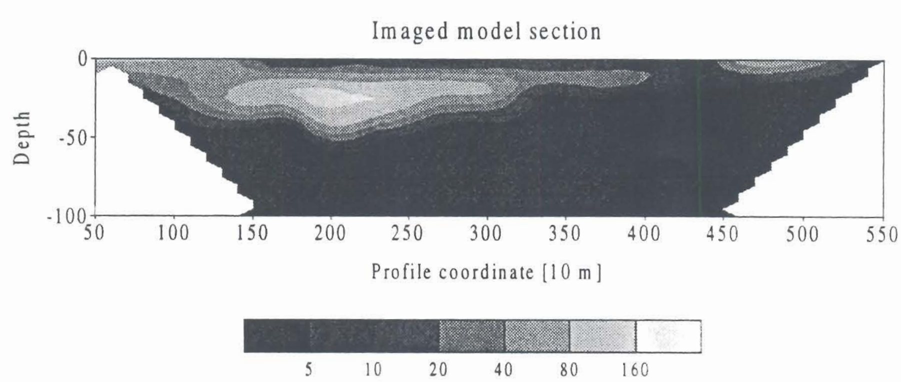

Fig. 5. An imaged model section from a TEM profile for the detection of the salt water horizon on the island of Rømø, Denmark.

6 Conclusion

The imaging algorithm is fast, robust, fully automated, and requires no initial model. The computation time, including the transformation from dH/dt to H-field, is approximately 0.5 sec/sounding/Mflop, which is 2-3 orders of magnitude faster than conventional least squares iterative inversion. The imaging produces models which fit the original data typically within 5-15%.

The imaged models may be used as very good input models to an iterative least squares inversion program, can be implemented as an on-line interpretation in TEM instruments, and the imaging procedure lends itself readily to AIM strategies (Oldenburg 1991). Contoured model sections based on imaged models from soundings along profile lines give a very fast insight in the subsurface conductivity distribution.

The principles of the imaging algorithm based on the Fréchet kernel can be extended to the 2D and 3D case of transient data. In fact, the idea of an instantaneous scaling of the Fréchet kernel according to some "average value" of the investigated parameter is applicable in other areas, as long as an "average parameter" can be defined and if the Fréchet kernel depends on the investigated parameter.

References

Boerner, D.E., and West, G.F., 1989. A generalized representation of the electromagnetic fields in a layered earth. Geophysical Journal, 97, 529-547.

Christensen N.B., 1995. Imaging of central loop transient electromagnetic soundings. Journal of Environmental and Engineering Geophysics, vol. 0, No. 1, 53-66.

Christensen, N.B., and Sørensen, K.I., 1994. Integrated use of electromagnetic methods for hydrogeological investigations. Proceedings of the Symposium on the Application of Geophysics to Engineering and Environmental Problems (SAGEEP), Boston, March 1994, p 163-176.

Macnae, J., and Lamontagne, Y., 1987. Imaging quasi-layered conductive structures by simple processing af transient electromagnetic data. Geophysics, 52, 545-554.

Oldenburg, D.W., and Ellis, R.G., 1991. Inversion of geophysical data using an approximate inverse mapping. Gephys. J. Int. 105, 325-353.

Raiche, A.P., Jupp, D.L.B., Rutter, H., and Vozoff, K., 1985. The joint use of coincident loop transient electromagnetic and Schlumberger sounding to resolve layered structures. Geophysics, 50, 1618-1627.

Smith, R.S., Edwards, R.N., and Buselli, G., 1994. An automatic technique for presentation of coincident-loop, impulse-response, transient, electromagnetic data. Geophysics, 59, 1542-1550.

Spies, B.R., and Eggers, D.E., 1986. The use and misuse of apparent resistivity in electromagnetic methods. Geophysics, 51, 1462-1471.

Spies, B.R., and Frischknecht, F.C., 1991. Electromagnetic Sounding. In: M.N. Nabighian (ed.), Electromagnetic methods in Applied Geophysics, Investigations in Geophysics, Vol. 2A, SEG.

Sørensen, K.I., Effersø, F., and Christensen, A.J..1995. Pulled array transient electromagnetic method (PA-TEM). SAGEEP conference, Orlando, p 899-903.

Sørensen, K.I., 1996. Pulled array continuous electrical profiling, PA-CEP, First Break, in press.